



Metabolic and Immune Markers for Precise Monitoring of COVID-19 Severity and Treatment

André F. Rendeiro^{1,2}, Charles Kyriakos Vorkas^{3†}, Jan Krumsiek^{1,2}, Harjot K. Singh³, Shashi N. Kapadia³, Luca Vincenzo Cappelli⁴, Maria Teresa Cacciapuoti⁴, Giorgio Inghirami⁴, Olivier Elemento^{1,2*‡} and Mirella Salvatore^{3,5*‡}

OPEN ACCESS

Edited by:

Julia Kzhyshkowska,
Heidelberg University, Germany

Reviewed by:

Alessia Vignoli,
University of Florence, Italy
Milena Sokolowska,
University of Zurich, Switzerland

*Correspondence:

Olivier Elemento
ole2001@med.cornell.edu
Mirella Salvatore
mis2053@med.cornell.edu

†Present address:

Charles Kyriakos Vorkas,
Division of Infectious Diseases,
Renaissance School of Medicine,
Stony Brook University, Stony Brook,
NY, United States

‡These authors share
senior authorship

Specialty section:

This article was submitted to
Viral Immunology,
a section of the journal
Frontiers in Immunology

Received: 05 November 2021

Accepted: 20 December 2021

Published: 12 January 2022

Citation:

Rendeiro AF, Vorkas CK, Krumsiek J, Singh HK, Kapadia SN, Cappelli LV, Cacciapuoti MT, Inghirami G, Elemento O and Salvatore M (2022) Metabolic and Immune Markers for Precise Monitoring of COVID-19 Severity and Treatment. *Front. Immunol.* 12:809937. doi: 10.3389/fimmu.2021.809937

¹ Institute for Computational Biomedicine, Department of Physiology and Biophysics, Weill Cornell Medicine, New York, NY, United States, ² Caryl and Israel Englander Institute for Precision Medicine, Weill Cornell Medicine, New York, NY, United States, ³ Department of Medicine, Weill Cornell Medicine, New York, NY, United States, ⁴ Department of Pathology and Laboratory Medicine, Weill Cornell Medicine, New York, NY, United States, ⁵ Department of Population Health Sciences, Weill Cornell Medicine, New York, NY, United States

Deep understanding of the SARS-CoV-2 effects on host molecular pathways is paramount for the discovery of early biomarkers of outcome of coronavirus disease 2019 (COVID-19) and the identification of novel therapeutic targets. In that light, we generated metabolomic data from COVID-19 patient blood using high-throughput targeted nuclear magnetic resonance (NMR) spectroscopy and high-dimensional flow cytometry. We find considerable changes in serum metabolome composition of COVID-19 patients associated with disease severity, and response to tocilizumab treatment. We built a clinically annotated, biologically-interpretable space for precise time-resolved disease monitoring and characterize the temporal dynamics of metabolomic change along the clinical course of COVID-19 patients and in response to therapy. Finally, we leverage joint immuno-metabolic measurements to provide a novel approach for patient stratification and early prediction of severe disease. Our results show that high-dimensional metabolomic and joint immune-metabolic readouts provide rich information content for elucidation of the host's response to infection and empower discovery of novel metabolic-driven therapies, as well as precise and efficient clinical action.

Keywords: COVID-19, metabolism, immunology, infection biology, precision medicine

INTRODUCTION

The pandemic caused by infection with the severe acute respiratory coronavirus type 2 (SARS-CoV-2) has infected more than 218 million people worldwide as of August 2021, caused more than 4.5 million deaths (1), and strains health systems on an unprecedented scale. The most common manifestations of COVID-19 are fever, cough, and dyspnea (2, 3), but thromboembolic events and other organ involvement are also common in patients with severe disease (2, 4, 5). Molecularly, severe COVID-19 disease is characterized by uncontrolled inflammatory syndrome caused by immune system hyperactivation (6–11). The most effective treatments are thus based on general immunosuppression with glucocorticoids (12) or neutralization of the pro-inflammatory interleukin 6 (IL-6) with tocilizumab (13).

Several laboratory tests such as albumin (14), CRP (15), lymphocyte abundance (16–19), IL-6 (20), and the fibrin degradation product D-dimer (21) have been used to monitor COVID-19, with their levels variably associated with disease severity. While these routinely available assays may have some clinical use in disease prognostication, they depict an incomplete landscape of pathophysiological changes associated with COVID-19. However these tests are mostly a readout of the inflammatory state and do not capture a wide but still interpretable view of the physiological state of COVID-19 patients. One possible approach is to increase the dimensionality of the system by the use of mixed-modality profiling such as the combination of immune population quantification and circulating cytokine levels (22, 23). While much work has been done on the characterization of the host immune response through cytometric or serological methods, characterization of the metabolic state of COVID-19 patients has just begun (24–28).

There are several lines of evidence demonstrating the importance of metabolic species - in particular lipids - during viral infection. Lipids are structural components of the host's cellular and organellar membranes, taking an active role in crucial cellular functions such as molecular trafficking, but are also of importance during viral attachment, internalization, packaging and release (29, 30). In animal models, it has been shown that cholesterol composition of membrane lipid rafts underpins the infectivity of SARS-CoV-2 (31). Beyond its structural functions, lipids are also crucial for energy supply and intracellular signalling (32, 33). It is plausible that viral-induced changes in host metabolism during COVID-19 in metabolites such as glucose and lipids (34) may be beneficial for the infection, by altering intracellular signaling and conditioning immune response. The host metabolome - lipids in particular - have therefore been proposed as potential biomarkers of COVID-19 disease severity (35), and as therapeutic targets to counteract excessive immune activation. Nuclear magnetic resonance (NMR) spectroscopy applied to the measurement of metabolites provides a great balance between precise and reproducible measurements, the breadth of analytes measured, and the logistical efforts necessary for data production (36–38). Importantly, it is also capable of discerning different lipid species in circulating lipoprotein particles.

In this work, we use NMR spectroscopy to identify changes in serum metabolome composition of COVID-19 patients that are associated with disease severity and tocilizumab treatment, and provide a method for precise disease monitoring, patient stratification, and early prediction of severe disease based on joint immuno-metabolic measurements.

RESULTS

Longitudinal NMR Metabolomics of COVID-19 Patient Plasma

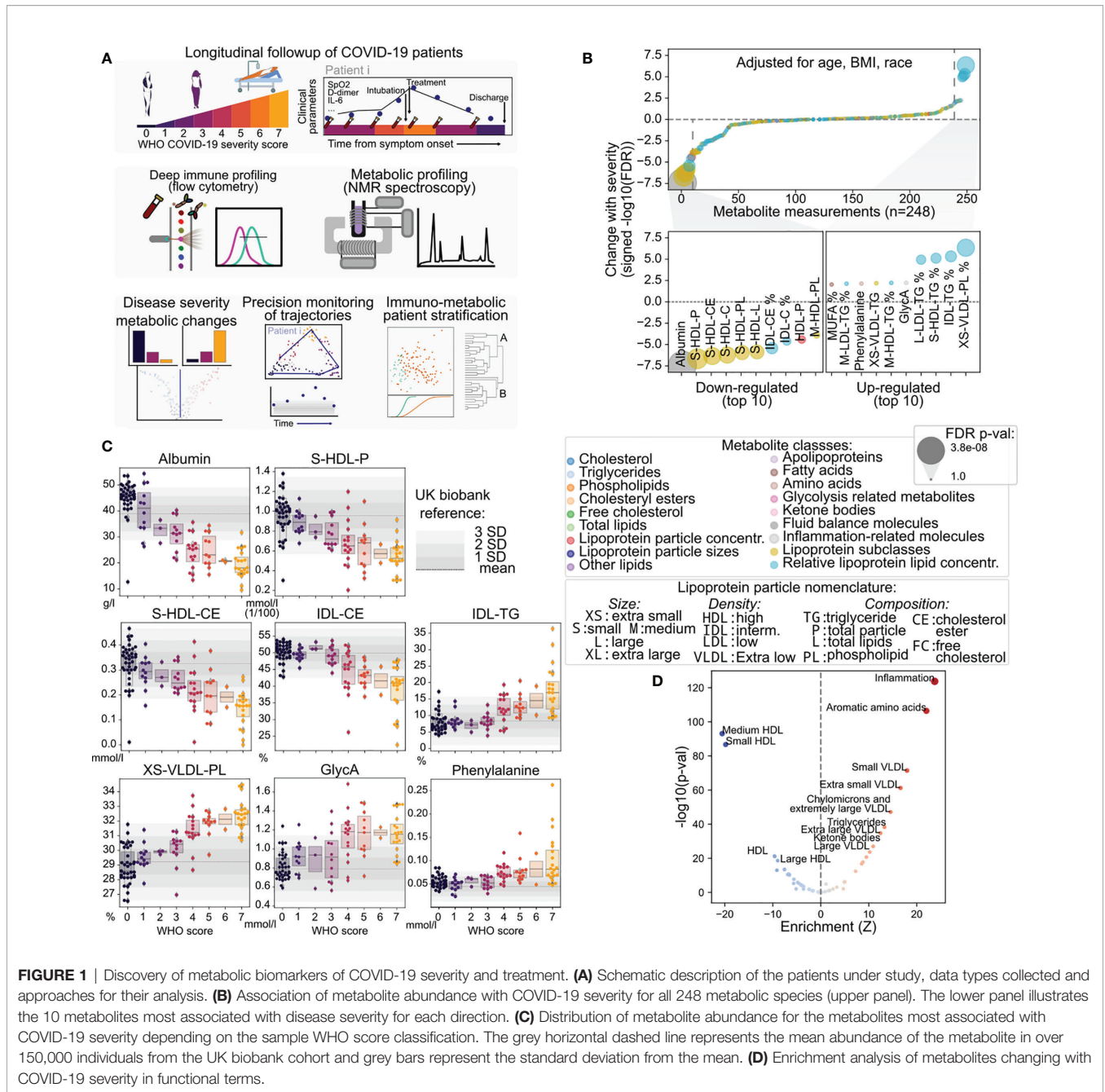
We conducted an observational study of 75 individuals with acute or convalescent COVID-19 that were treated at New York Presbyterian Hospital and Lower Manhattan Hospitals, Weill

Cornell Medicine as in- or out-patients between April and July 2020. The disease was categorized using World Health Organization disease severity scale for the prognostication of COVID-19 patients (39) (henceforth referred to as “WHO score”), which use clinical events such as patient admittance, amount of supplemental oxygen needed, or the need for mechanical ventilation (**Figure 1A** and **Table 1**). Serum samples were collected at hospital admission, when permissible approximately every 7 days thereafter, and for convalescent patients as outpatients at least 90 days from symptom onset (109 samples from 75 patients, 32 convalescent). Of all patients, 35 (47%) presented with low to mild disease severity, and 30 (40%) with moderate to severe disease. We also collected serum from healthy, COVID-19 negative donors ($n = 9$). The median age of COVID-19 patients was 53 years, which was comparable with that of healthy donors (51 years) (**Table 1** and **Table S1**).

We performed targeted high throughput NMR-based detection of metabolites in circulating blood serum (Nightingale Health Ltd.) (**Figure 1A** and **Tables S2, S3**). The NMR assay detected 168 metabolite species in absolute molar quantities, and 81 additional measurements of relative proportions covering diverse metabolic species such as lipids and fatty acids, apolipoproteins, amino acids, ketone bodies, and other molecules with known prognostic value across various diseases such as albumin, creatinine, and apolipoprotein levels (40–42) (**Figures S1A–C**). The panel is dominated by the diversity of lipids and by lipoprotein-associated lipid species which were fractionated based on their relative density and size (**Figures S1D–F**). Overall, measurements of the metabolic species had excellent reproducibility and high signal-to-noise ratio (**Figures S1G–H**). Upon relating the abundance levels of all metabolite species across all samples, we find that metabolites were heavily co-regulated (**Figure S1I**).

Metabolic Changes Associated With COVID-19 Severity

In order to identify the metabolic features associated with COVID-19 outcome, we leveraged linear mixed effect models to explain COVID-19 disease severity as a function of metabolite levels independently from patient age, gender, race, and body mass index (BMI) (**Figure 1B** and **Figures S2A, B**). While most of the 249 metabolite species showed no association with disease severity as measured by the WHO score, we found significant associations for 56 metabolites ($p < 0.05$, adjusted for multiple testing with the Benjamini Hochberg False Discovery Rate (FDR) method), which were dominated by lipid and lipoprotein subclasses (**Table S4**). Specifically, we found that albumin, high-density lipoprotein (HDL) and small HDL particle species, as well as the cholesteryl-ester component of HDL and intermediate-density lipoproteins (IDL) declined proportionally with the increase in WHO score, with steeper decline in the most severe cases (**Figure 1C**). On the other hand, extra small, very low-density lipoprotein (VLDL) particles with increased phospholipids component and extra-small VLDL, IDL, LDL and HDL with increased triglycerides were correlated with increased severity. Additional variables associated with



increased disease severity were acetylated glycoproteins (GlycA) - a spectroscopic marker of systemic inflammation (43), phenylalanine, and fraction of monounsaturated fatty acids (MUFA). We also observed a significant association of acetoacetate, 3-hydroxybutyrate, phenylalanine, and the ratio of apolipoprotein B to A1 (ApoB/ApoA1) to disease severity (Figure S2C). Of note, the levels of many of the mentioned metabolites in severe COVID-19 (WHO score 4-7) were higher by more than three standard deviations than the mean of a large non-COVID population from the UK Biobank (150,000 samples) (44, 45), illustrating the degree of metabolic disarray

in the serum of COVID-19 patients with severe disease. These results are also in agreement with previous reports (24, 46).

Additionally, we performed enrichment of the changes associated with COVID-19 severity in metabolite groups based on their biophysical properties and known physiological roles. This analysis revealed increased levels of inflammation markers, amino acids and triglycerides, but above all confirmed the deep unbalance in lipoprotein composition, size, and density (Figure 1D and Figure S3A), where increased severity is associated with decreased lipoprotein density and increased size, which are in line with the increased triglyceride content of

TABLE 1 | Demographic and clinical characteristics of the cohort.

	Patient group					P-value
	Uninfected (n = 9)	Low (n = 39)	Mild (n = 7)	Moderate (n = 11)	Severe (n = 18)	
Age	48.22 (18.41)	42.74 (10.88)	58.22 (12.33)	67.65 (9.94)	68.21 (13.04)	2.17E-11*
Race						1.85E-01
Asian	1	4	1	1	6	
Black	0	2	0	3	1	
Other	0	1	0	0	1	
White	8	31	6	6	10	
Sex						9.50E-01
Female	5	18	3	5	7	
Male	4	21	4	6	11	
Obesity						2.51E-02*
Nonobese	8	19	4	1	9	
Overweight	0	8	0	5	5	
Obese	1	5	3	5	4	
Body mass index	30.77 (8.89)	27.19 (4.17)	27.48 (4.55)	30.33 (5.99)	27.42 (4.89)	2.40E-01
Days of symptoms before admission		7.17 (9.6)	10.0 (10.57)	8.29 (5.8)	7.77 (4.26)	7.02E-01
Underlying pulmonary disease		3	1	1	5	5.84E-01
Hospitalization		3	6	11	18	1.71E-10*
Intubation		0	0	0	10	2.00E-08*
Tocilizumab treatment		0	0	1	9	1.65E-03*
Death		0	0	0	7	1.25E-05*
Total bilirubin	0.5 (0.17)	0.8 (0.63)	0.68 (0.25)	0.62 (0.2)	0.63 (0.31)	8.44E-01
ALT	18.33 (12.86)	28.0 (21.71)	40.25 (40.72)	41.0 (13.89)	47.65 (54.18)	2.23E-01
AST	16.0 (6.24)	50.0 (59.35)	43.25 (31.71)	32.5 (15.41)	48.16 (49.09)	1.30E-01
Creatinine	1.18 (0.07)	0.76 (0.19)	0.84 (0.16)	0.84 (0.3)	2.07 (2.13)	3.22E-01
CRP	10.8 (NAN)	NAN	2.42 (2.13)	7.58 (8.91)	12.47 (9.58)	1.39E-01
Hemoglobin	8.9 (2.38)	12.22 (3.21)	10.41 (2.11)	11.58 (1.47)	9.91 (2.38)	8.58E-02
Hematocrit	26.87 (6.5)	37.58 (8.82)	31.0 (5.82)	35.02 (4.33)	31.57 (11.03)	1.03E-01
LDH	272.0 (46.67)	NAN	286.67 (93.39)	301.0 (112.56)	506.71 (214.17)	1.57E-02*
RDWCV	17.33 (2.47)	16.4 (3.92)	15.42 (2.32)	24.5 (22.12)	16.72 (3.23)	6.94E-01
MCV	89.57 (2.97)	87.18 (6.59)	95.46 (8.33)	76.41 (24.12)	92.89 (4.94)	8.04E-05*

For simplicity we aggregate patients based on an assessment of overall disease severity along the course of disease. Float-point values with parenthesis in front indicate the mean and standard deviation within the patient group. Integers indicate the total count of individuals. Values between hyphens indicate the minimum and maximum values within the group. NAN indicates the measurements were not available. The independence between these patient groups and categorical variables was assessed with a Chi-squared independence test, and for numerical variables with a Kruskal-Wallis one-way analysis of variance. ALT, alanine aminotransferase; AST, Aspartate transaminase; CRP, C-reactive protein; LDH, lactate dehydrogenase; RDWCV, Red Cell Distribution Width; MCV, mean corpuscular volume. Asterisk indicates significance at $\alpha < 0.05$.

the particles. One exception is extra-small VLDL particles (3–6 nm) which are also increased in severe disease. Taken together, the observed changes reveal considerable metabolic changes in COVID-19 patients dependent on disease severity. As a comparison, we investigated the association of routinely collected clinical biomarkers with COVID-19 severity in our cohort and found that only lactate hydrogenase (LDH) was significantly associated with disease severity (**Figures S3B, C**), while biomarkers of overall metabolic homeostasis such as aspartate aminotransferase (AST) and alanine aminotransferase (ALT) were not.

Effect of Tocilizumab Treatment on the Metabolome of COVID-19 Patients

Among the therapeutic options for COVID-19, Tocilizumab, an inhibitor of the pro-inflammatory interleukin-6 (IL-6) was used in COVID-19 patients with elevated inflammatory markers and rapidly escalating oxygen requirements. In our cohort, 10 (12%) patients were treated with Tocilizumab. To assess metabolic changes associated with tocilizumab treatment, we fit a linear model on the time since treatment with age, gender, race, BMI, and disease severity as covariates. Several metabolite species were significantly associated with tocilizumab treatment (**Figure 2A**

and **Figures S4A–C, Table S5**), in particular an increase in VLDL particles but also in their cholesterol content (both free and esterified), reduction of valine levels, triglyceride content of VLDL, and ratio of the polyunsaturated fatty acids (PUFA) Omega 6 to 3 - a ratio associated with the pathogenesis of various diseases (47, 48) (**Figure 2B**). However, we also observed metabolite species that were significantly changed with COVID-19 severity with no apparent change with tocilizumab treatment (**Figures 2A, B, and Figures S4E–G**). Across all metabolite species, we observed a trend for patients treated with Tocilizumab to have a metabolic state more similar to patients with milder disease over time (**Figure 2C**), which suggests that the administration of Tocilizumab could contribute to a partial rescue of some of the effect of severe disease on the metabolism of COVID-19 patients.

Precise Monitoring of COVID-19 Clinical Trajectories by Intra-Patient Metabolome Dynamics

Given the sensitivity of targeted NMR metabolomics to detect changes of disease severity in COVID-19 patients, we hypothesized that these data could be used as a rich, multivariate measurement of disease severity grounded in

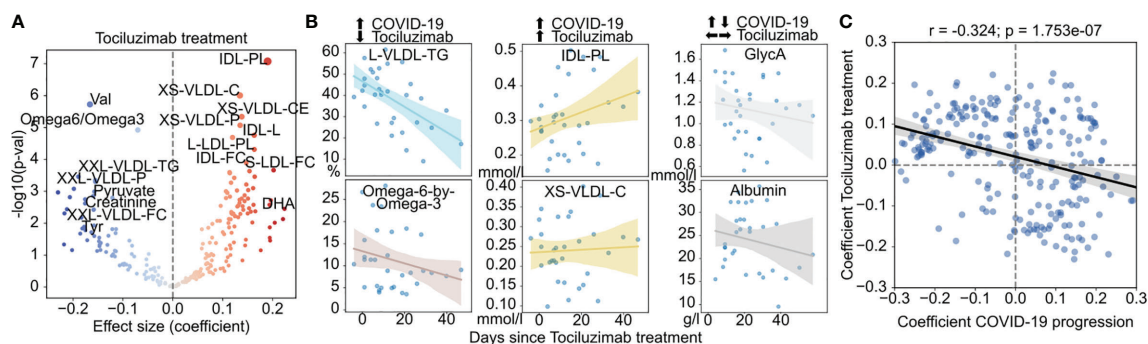


FIGURE 2 | Effect of tocilizumab treatment on the metabolism of COVID-19 patients. **(A)** Association of metabolite abundance with the time since tocilizumab treatment. The coefficient values refer to the change per day in relation to the mean. **(B)** Abundance of metabolites with discordant (left), concordant (center) or indifferent (right) change between COVID-19 severity and tocilizumab treatment for treated patients. **(C)** Comparison of the coefficients of change in COVID-19 severity (x-axis) and effect of tocilizumab treatment over time (y-axis). The black regression line indicates a overall linear trend across all metabolites.

metabolic data. First, to understand the temporal dynamics of the metabolism of COVID-19 patients, we created a two-dimensional latent space using diffusion maps on the abundance of the metabolites across all samples (**Figure 3A**). This space, made of diffusion components (DC) was largely driven by the severity of disease and clinical outcomes associated with it such as hospitalization, intubation, and death, and the time since symptom onset (**Figure 3A** and **Figures S5A, B**). This allowed us to use the distribution of clinical attributes on the space to inform of the relative risk of adverse outcomes (including hospitalization, intubation and death) for patients (**Figure 3A**, right and **Figure S5C**).

Importantly, this relationship is largely independent of the statistical method used to construct a latent space (**Figure S5D**). Second, we used pseudotime to derive a direction of progression through the latent space for each patient over multiple timepoints. This allowed us to order samples based on their predicted trajectory along the overall course of disease severity (**Figure 3B**). Finally, we were able to observe the trajectory of each patient along the latent space, and by weighting the amount of change by the time between timepoints we could derive a measure of speed of change of metabolome for each patient, and an aggregate measure of how much the metabolome changed over time (**Figures 3C–E**). For example, patients 23 and 24 have similar trajectories at start - starting at an area of intermediate risk and progressing to an area of highest severity -, but later move to an area occupied most by healthy and convalescent individuals or remain in the area of highest risk, respectively (**Figure 3D**). These divergent trajectories are apparent in the predicted relative risk from metabolic data, while a single marker such a GlycA tends to inform only of one specific aspect of the metabolome (inflammation) (**Figure 3E**).

The longitudinal aspect of the data and its reduction to a single landscape further allowed us to study the temporal kinetics of disease severity and recovery (**Figure 3G**). We hypothesized that the overall speed of each patient along their timeline could be related to their clinical status. We observed that different patients can have largely different speeds of metabolic change

during their clinical timeline (**Figure 3G–H**), and sought to identify a clinical parameter that would be associated with that change (**Figure 3I**). We discovered that the overall speed of metabolic change along the whole timeline of the patient was related with the overall disease severity of the patients and whether the patient was hospitalized (**Figure 3J**). This observation suggests that higher rates of metabolic changes over time are an index of the complex interactions between viral infection, treatment, and individual host response, and may translate into (or reflect) a worse overall outcome for the patients. Taken together, our pseudo-temporal analysis of the metabolomics dataset revealed a dynamic landscape of metabolic change within patients over time, which can be used to measure disease progression in near-real time.

Integration of Immune and Metabolic Data for Patient Stratification

Since metabolic requirements underpin immune activation (49, 50) which is needed for response to infection (51–53), and immune effectors are known to regulate key enzymes in lipid metabolism (54, 55) we sought to uncover the relationship between metabolite abundance and immune system composition by performing regularized regression on the NMR metabolomics and flow cytometry immune profiling datasets (56) (**Figure 4A**). This resulted in a map of interactions between metabolites and immune populations, of which **Figure 3A** illustrates the strongest. Interactions between immune and metabolic variables could be largely categorized in two groups: i) positive association (**Figure 4A** red in the heatmap): immune variables changing in the same direction as metabolic variables; ii) negative association (**Figure 4A** blue in the heatmap): increase in metabolic variables correlated with decrease in immune variables or vice-versa. For example, the decrease in Albumin levels during COVID-19 was matched with the increase in polymorphonuclear myeloid-derived suppressor cells (PMN-MDSC); total T-cell abundance was related to the fraction of medium size HDL, where both variables decrease with COVID-19 severity. The immune checkpoint inhibitors Lag3 and Tim3

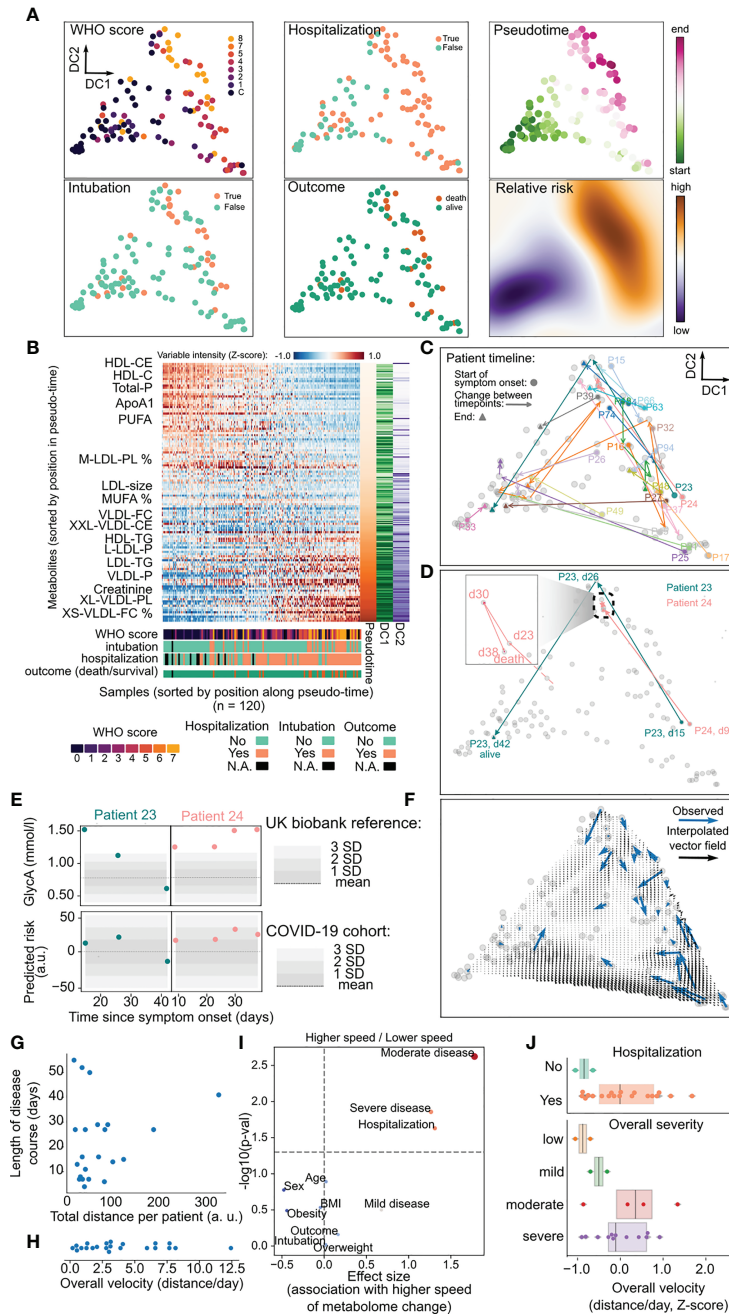


FIGURE 3 | Use of metabolic data for precise disease monitoring. **(A)** Latent representation of metabolic data for all samples in two dimensions using diffusion maps, from which diffusion components (DC) are derived. In the first two panel columns samples are colored by their value of WHO score, whether the patient was hospitalized, intubated and their survival. The rightmost column indicates the position of each sample within the inferred pseudotime and the relative risk for the whole two-dimensional space. **(B)** Heatmap with relative abundance of metabolites for all the samples where both axes are sorted by their relative position along the inferred pseudotime. The lower part of the plot indicates the values of clinical parameters for every sample. **(C)** Trajectory of each patient across the latent space during their clinical course starting with the day of symptom onset. Patients with at least three samples are colored distinctly while the remaining are colored in gray. **(D)** Particular trajectories for patients 23 and 24 as in c). The inset illustrates the stagnated course of patient 24. dN = n days since symptoms onset. **(E)** Values of GlycA and the predicted risk for patients 23 and 24 along the clinical trajectories of each patient. The shaded area in the GlycA plots represents the distribution of that metabolite in the UK biobank cohort, while the shaded area for predicted risk represents the distribution of the COVID-19 cohort. **(F)** Vector field of velocities in the latent space interpolated from the observed velocity vectors for all patients (blue). **(G)** Relationship between total distance moved per patient in the latent space over the whole clinical course and its length in days from symptom onset. **(H)** Distribution of average velocities across the whole clinical timeline for every patient. **(I)** Association analysis between clinical variables and the average velocity of each patient. *p*-values have been adjusted with the Benjamini-Hochberg FDR method. **(J)** Illustration of differences between patient velocities and their hospitalization or overall disease severity across the whole clinical timeline.

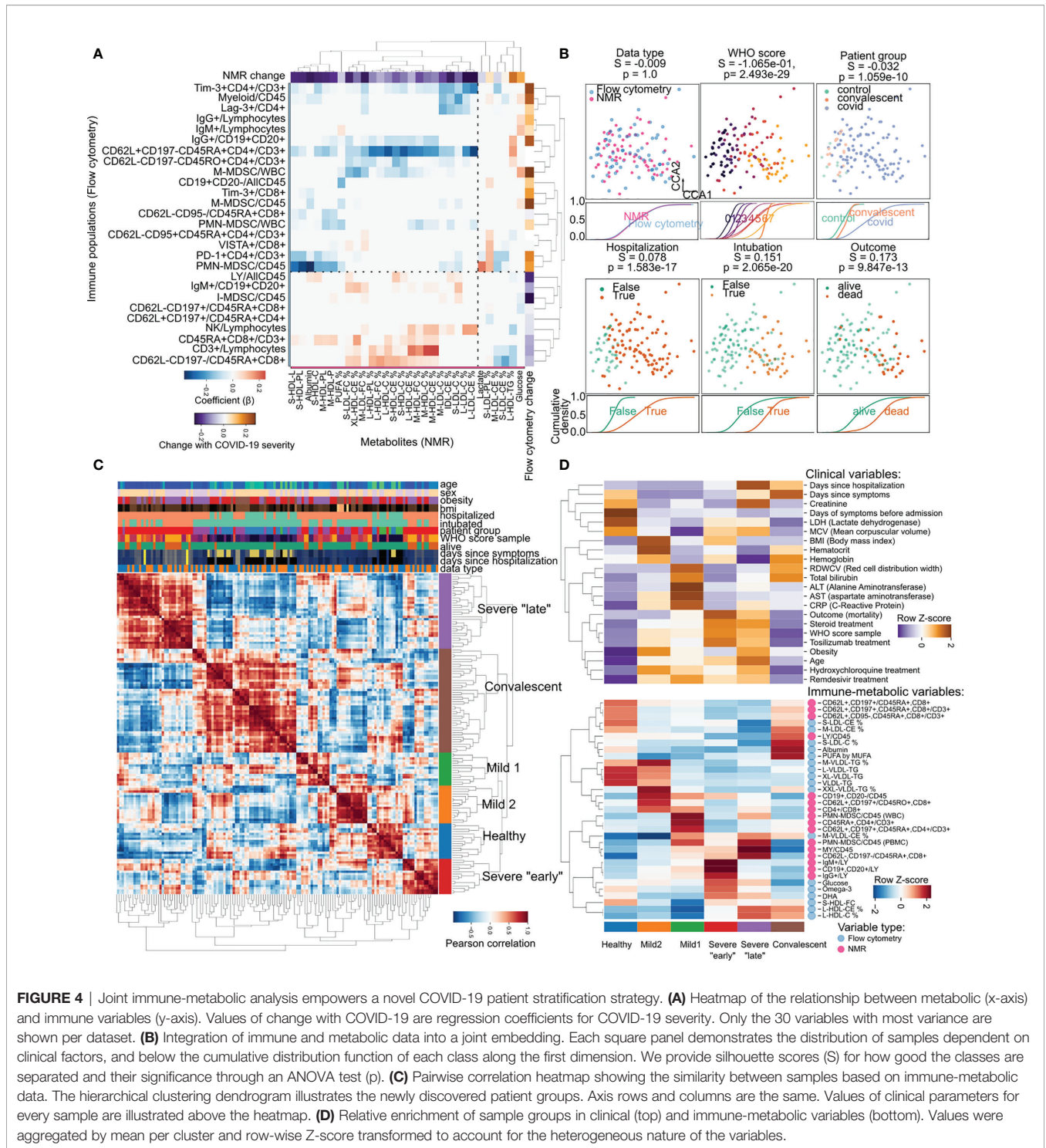


FIGURE 4 | Joint immune-metabolic analysis empowers a novel COVID-19 patient stratification strategy. **(A)** Heatmap of the relationship between metabolic (x-axis) and immune variables (y-axis). Values of change with COVID-19 are regression coefficients for COVID-19 severity. Only the 30 variables with most variance are shown per dataset. **(B)** Integration of immune and metabolic data into a joint embedding. Each square panel demonstrates the distribution of samples dependent on clinical factors, and below the cumulative distribution function of each class along the first dimension. We provide silhouette scores (S) for how good the classes are separated and their significance through an ANOVA test (p). **(C)** Pairwise correlation heatmap showing the similarity between samples based on immune-metabolic data. The hierarchical clustering dendrogram illustrates the newly discovered patient groups. Axis rows and columns are the same. Values of clinical parameters for every sample are illustrated above the heatmap. **(D)** Relative enrichment of sample groups in clinical (top) and immune-metabolic variables (bottom). Values were aggregated by mean per cluster and row-wise Z-score transformed to account for the heterogeneous nature of the variables.

which we previously described increasing with COVID-19 severity showed interactions with the fraction of cholesterol in LDL particles, themselves decreasing with COVID-19 severity. While many of these potential interactions are not yet described, and many are indirect, there are also specific examples of direct interactions, such as HDL interference with the potential of T cells to produce some cytokines, through a proposed mechanism

of direct binding (57). The relationships between the two datasets made us hypothesize that it could be possible to establish a patient-centric view of the immune-metabolic landscape during COVID-19. Towards that end, we employed regularized Canonical Correlation Analysis (rCCA) to integrate both NMR and flow cytometry datasets in a common latent space (Figure 4B). In this new space, samples clustered based on

disease severity and its associated clinical outcomes regardless of dataset origin (**Figure 4B**). This allowed us to build a novel way to stratify patients based on both immune and metabolic data by hierarchical clustering of the pairwise similarity between patient samples (**Figure 4C**). In this classification we could identify six groups: one with predominantly healthy samples (11% of all samples); two groups of patients with mild disease (10 and 12% respectively); two groups mostly containing patients with severe disease (one with samples collected close to symptom onset, and the other later (11 and 24% respectively); and finally a group of samples from mostly convalescent patients (32%) (**Figure 4C**). The six groups were characterized by distinct clinical parameters and abundance of immuno-metabolic species (**Figure 4C**). For example, the two groups of mild disease could be distinguished by distinct BMI, liver enzyme levels, and triglyceride content of lipoproteins. Additionally, the “late” severe disease group had creatinine levels markedly higher than the “earlier” severe group, as opposed to B-cell expression of immunoglobulins G and M (IgG/IgM) which was highest in “early” disease and later decreased (**Figure 4D**).

DISCUSSION

Here we present longitudinal immuno-metabolic data on a cohort of COVID-19 patients representative of the whole range of disease severity. We show that patient metabolism during disease is quite dynamic, reflecting disease progression and treatment. Consistent with a previous report, increased markers of systemic inflammation correlated with COVID-19 severity (25). More importantly, we identified a deep alteration of the lipoprotein particles levels and composition: increased triglyceride content and VLDL, decrease of HDL, percentage of cholesterol/cholesteryl esters in HDL, and IDL were associated with severe disease. Previous studies have proposed a decrease in cholesterol and increase in triglycerides (24, 27, 46) as markers of severe COVID-19. In our study we confirm these findings and further describe the deep modification in the lipid metabolism and composition of lipoprotein and fatty acid associated with the disease. This is reminiscent of a metabolic state known to predispose to cardiovascular disease (58–60) and could be related to the thrombotic events observed in COVID-19 patients with severe disease (2, 4, 5, 61, 62). Furthermore, we develop groundwork for the future development of tools that can precisely monitor COVID-19 patient trajectories using metabolic data, potentially enabling risk assessment on a continual fashion. We must nonetheless acknowledge the following limitations to our study: i) our cohort is relatively small especially in comparison with large repositories such as the UK biobank; ii) our cohort is also skewed to have more patients with longitudinal follow-up for patients with severe disease - this is at least in part due to the natural dynamic severe disease having a longer recovery period; iii) our analysis of the interaction between the immune system and metabolome is purely correlational, as we can't infer causality between the presence or activity of an immune cell type with the abundance of a metabolite.

It is plausible that cytokine modulation of key metabolic enzymes or energy usage by the immune system during acute infection are a major source of the metabolic changes associated with COVID-19 progression (63). It has been shown for COVID-19 specifically that in T-cells cholesterol interacts with sphingolipids in membrane rafts in a manner that is dependent on the saturation state of the fatty acids (31), and more generally that lipid raft formation has a crucial role in the cytotoxic activity of CD8 T-cells (64–66). The increase in triglyceride composition of lipoprotein particles and their saturation state we observed with increased disease severity could result in altered immune function. Evidence for that has been seen in the regulation of immune checkpoint proteins such as CTLA4 in MDSCs by intracellular PUFA levels in cancer models (67). Another example is the shift between energy sources in T effector cells from glucose to aminoacids which is required for proliferation and cytotoxic activity (51–53).

Additional evidence of immune influence on metabolism in our data is the fact that tocilizumab - a monoclonal antibody that inhibits the binding of the pro-inflammatory cytokine IL-6 to its receptor - partially rescues the effect of disease severity at the metabolic level (**Figure 2C**). This is in agreement with a previous study reporting a similar rescue effect of Tosiluzimab on COVID-19 associated metabolic alterations (27). This reinforces the idea that metabolic changes during COVID-19 are likely to be at least partially driven by the immune system either directly through regulation of key metabolic enzymes by cytokines, energy consumption of cytokine-secreting cells, or by the effect of immune cells on other tissues. At the same time, in our study BMI had a negligible influence on disease severity (**Figure S2A**), and biomarkers for liver function such as AST and ALT did not show significant association with disease severity (**Figures S3B, C**), making nutrition, obesity and liver dysfunction unlikely candidates to explain metabolic changes linearly associated with COVID-19 severity. Nonetheless, the contribution of these and other factors should be further explored in future studies with larger sample sizes and complete measurements of well-established clinical significance such as D-dimer.

The immune-metabolic crosstalk taking place during COVID-19 progression suggests the future potential use of metabolites to control disease through direct modulation of specific steps of lipid metabolism at the immune level. In that light, having precise methods for disease monitoring that capture both metabolism and immune system states would be extremely useful. In this study we develop a method for patient monitoring using NMR spectroscopy of metabolites from blood sera (**Figure 3**) that is quantitative, does not rely on thresholds, and can be interpreted in terms of patient risk at any given time during the patient's clinical trajectory. Further development of our approach of joint immuno-metabolic classification of overall patient trajectories (**Figure 4**) could be used early in the course to tailor patient care and maximize allocation of medical resources.

Collectively, our study unveils the considerable metabolic disarray during COVID-19 progression which could open avenues for the development of metabolic-based therapies.

Further, by leveraging immuno-metabolic high-dimensional data, we provide novel methods for precise disease monitoring and stratification in order to effectively tailor clinical care to COVID-19 patients.

METHODS

Human Studies

Blood serum samples were collected at the New York Presbyterian Hospital/Weill Cornell Medicine. Experiments using samples from human subjects were conducted in accordance with local regulations and with the approval of the IRB at the Weill Cornell Medicine (IRB 20-03021645). No statistical methods were used to pre-determine sample size.

Targeted Metabolomics With Nuclear Magnetic Resonance

Venous blood was collected from donors without fasting in heparinized tubes at the indicated days. Samples were processed within 24 hrs from collection. Plasma was stored in aliquots at -80°C until use. Analytes were quantified from plasma samples using targeted high-throughput NMR metabolomics (Nightingale Health Ltd., Helsinki, Finland) using 100-350 μL aliquots. This platform provides simultaneous quantification of routine lipids, lipoprotein subclasses, fatty acids and their saturation, several low-molecular weight metabolites (amino acids, ketone bodies and glycolysis metabolites), as well as a set of clinically validated biomarkers associated with different metabolic pathways relevant to human physiology in molar concentration units. One advantage of the platform is that biomarkers were quantified independently for each sample without information from reference samples in the same well-plate or same cohort, enabling absolute quantification. In total, 249 measures were produced with 148 in absolute molar quantification. This platform (same metabolite measurements) has been extensively described and validated across large cohorts (68, 69).

Analysis of Nuclear Magnetic Resonance Data

In order to categorize the NMR analytes biophysically and functionally, we used data distributed by the *ggforestplot* package (36) (<https://github.com/NightingaleHealth/ggforestplot>) and complemented them with variables representing lipoprotein particle size and density according to the variable names. Values of replicability per analyte were extracted from measurements of technical replicates performed by Nightingale Health Ltd. publicly available at: https://biobank.ndph.ox.ac.uk/showcase/showcase/docs/nmrm_app2.pdf. Summary statistics for metabolite species abundance at population scale were obtained from the publicly available resource showcase of the UK biobank (44) (<https://biobank.ndph.ox.ac.uk/ukb/>) by querying field IDs 23400 to 23578. In order to build data-driven groups of variables, we used a standardized and centered matrix of features with absolute measurements only, and computed a nearest neighbor graph using 15 neighbors as the size of the local neighborhood (*scanpy.pp.neighbors*).

These were used as input for UMAP (*scanpy.tl.umap*) and clustered using the Leiden algorithm (*scanpy.tl.leiden*), both with default parameters using Scanpy (70).

To identify variables associated with COVID-19 severity, we performed linear regression using a mixed effect model. The model used age, gender, and body mass index (BMI) as covariates, with the WHO score per sample as the dependent variable, and fixed effects for each patient. To identify variables associated with tocilizumab treatment, we performed linear regression with a generalized linear model. The dependent variable was the time in days since treatment began, and only samples of patients which received treatment were included. Covariates of age, gender, and body mass index (BMI) were also used. We ensured there was no collinearity between predictors by measuring their variance inflation factor using *statsmodels*. We fit the models for all variables, inspected the distribution of residuals and for the mixed effect model also compared the estimated coefficients to a generalized linear model with no blocking on patient, and to models not incorporating the covariates. We found that the estimated effect of COVID-19 severity between these models was highly similar ($r^2 = 0.985$). *p*-values were corrected for multiple testing using the Benjamini-Hochberg FDR method. To assess whether the group of features significantly associated with COVID-19 severity or tocilizumab treatment were enriched in any particular biophysical and functional classes, we performed enrichment analysis using the annotation classes of the metabolites and parametric analysis of gene set enrichment (71) (PAGE) as implemented in <https://github.com/afrendeiro/page-enrichment>.

Generation of a Latent Space for Precision Disease Monitoring

To establish a latent space embedding using the metabolomics data, we performed spectral embedding of the metabolomics data (*sklearn.manifold.SpectralEmbedding*). We also compared the results of this method to the following methods for dimensionality reduction: principal component analysis (PCA), non-negative matrix factorization (NMF), multidimensional scaling (MDS), non-linear dimensionality reduction through isometric mapping (Isomap), *t*-distributed stochastic neighbor embedding (72) (*t*-SNE), uniform manifold approximation and projection (UMAP), as implemented in *scikit-learn*, diffusion maps (DiffMap) as implemented in Scanpy (70), and minimum-distortion embedding (70, 73) (MDE) from the *PyMDE* package. Spectral embedding produces exactly the same results as diffusion maps (DiffMap) with default parameters if the input matrix is standardized and centered. To order variables along a gradient within the derived latent space across its two dimensions, we correlated the original features with each latent vector, scaled each to the unit range and multiplied the values of dimension 1 and 2. Then, to order samples along this gradient, we simply computed the correlation of each sample with the previously derived vector.

Inference of clinical parameters distribution within the latent space was done as previously (74): two bivariate gaussian kernel density estimators were fitted on the coordinates of the samples

with the difference being that one was weighted by the respective value of the sample in the clinical parameter. The final values are given by the difference between the two estimators. The compound measure of relative risk is the average of these estimations for the WHO score, hospitalization, intubation, and death.

To generate a vector field of patient movement through the latent space, we extracted vectors representing the movement of each sample at each timepoint by dividing the euclidean distance between points by the time between each two consecutive timepoints. Then, we interpolated these values across the two-dimensional latent space (*scipy.interpolate.griddata*). The total velocity of each patient in the space was calculated as the total distance over the length of the timeline (first to last NMR sample). To derive a score of COVID-19 severity for each sample, we also separated features dependent on the sign of the coefficients of the mixed effects model and calculated the difference in the mean of up-regulated features and mean down-regulated features scaled by their relative size.

Joint Analysis of Nuclear Magnetic Resonance and Flow Cytometry Datasets

In order to understand the relationship between metabolic variables and immune populations, we performed Ridge regression between the NMR and flow cytometry datasets with hyperparameter optimization using random search cross-validation (*sklearn.model_selection.RandomizedSearchCV*) for the alpha parameter sampled from a log-uniform distribution with parameters $a = 1e-20$, and $b = 1$ for 1000 iterations. The coefficients of the best model were highly regularized ($\alpha = 0.979196$) and were used to represent the relationship between metabolic and immune population variables.

To produce a joint embedding of metabolic and immune data for each patient timepoint, we employed regularized canonical correlation analysis (75) (RCCA) in the Python implementation *pyrcca*. We performed hyperparameter optimization with grid search cross validation using a number of canonical components between 4 and 8, and a regularization parameter between $1e-3$ and $1e3$. The best number of canonical components was 6 and the regularization parameter was 90. The separation of groups of samples dependent on clinical parameters was assessed with a silhouette score and an analysis of variance (ANOVA) test on the first 2 canonical components only.

To produce a stratification of patients based on the joint projection of the two datasets in the RCCA space by correlating samples in a pairwise fashion and extracting the first 6 splits of a dendrogram derived from hierarchical clustering of the correlation coefficients. The association of clinical or immune-metabolic variables with the derived patient groups was performed by fitting a linear model explaining those variables using the patient groups. In the case of immune-metabolic data, only the top 3 variables per group were chosen for visualization.

Software used: Python version 3.8.2, numpy (76) 1.21.0, scipy (77) 1.7.0, statsmodels (78) 0.12.2, scikit-learn (79) 0.24.2, scanpy (70) 1.8.0, pymde (73) 0.1.12, *pingouin* (80) 0.3.12, and *pyrcca* (75) 0.1.

CODE AVAILABILITY

Source code for the full data analysis of the study is available at the following URL: <https://github.com/ElementoLab/covid-metabolomics>.

DATA AVAILABILITY STATEMENT

The datasets presented in this study can be found in online repositories. The names of the repository/repositories and accession number(s) can be found in the article/**Supplementary Material**.

ETHICS STATEMENT

The studies involving human participants were reviewed and approved by Weill Cornell Medicine IRB 20-03021645. The patients/participants provided their written informed consent to participate in this study.

AUTHOR CONTRIBUTIONS

GI, OE, and MS planned the study. CKV, HKS, MS and SNK provided samples and clinical data. LVC and MTC processed samples. AFR performed analysis of the data with contributions from JK. GI, OE, and MS supervised the research. AFR, LVC, JK, OE, and MS wrote the manuscript with contributions from all authors. All authors contributed to the article and approved the submitted version.

FUNDING

AR is supported by a NCI T32CA203702 grant. OE is supported by NIH grants UL1TR002384, R01CA194547, and Leukemia and Lymphoma Society SCOR 7012-16, SCOR 7021-20 and SCOR 180078-02 grants. CV was supported by NIAID K08 AI132739 and a Potts Memorial Foundation Award.

ACKNOWLEDGMENTS

We would like to thank Karsten Suhre for his expertise on metabolic analysis.

SUPPLEMENTARY MATERIAL

The Supplementary Material for this article can be found online at: <https://www.frontiersin.org/articles/10.3389/fimmu.2021.809937/full#supplementary-material>

Supplementary Figure 1 | Characterization of the NMR metabolomics panel. **(A–C)** Composition of the panel dependent on the biophysical characteristics of the analytes from **A** to **C** with increased granularity. **(D, E)** Composition of the lipoprotein particle variables in the panel depending on their density **(D)** and size **(E)**.

(F) Absolute abundance of metabolites depending on their density or size. (G) Measures of reproducibility and signal-to-noise for all metabolites in the panel. (H) Relationship between mean and variance for all variables in the panel. (I) Pair-wise correlation of metabolite abundance.

Supplementary Figure 2 | Metabolic changes associated with COVID-19 severity. (A) Number of significant ($p < 0.05$ FDR) variables for a joint model of COVID-19 severity, patient age, BMI, and race. (B) Volcano plot of changes in metabolites associated with COVID-19 severity. (C) Heatmap of relative metabolite abundance for all samples where the axes have been sorted by the amount of change. (D) Abundance of metabolites with significant association with COVID-19 severity depending on WHO score.

Supplementary Figure 3 | Metabolic and clinical association of disease severity. (A) Distribution of log fold-changes in lipoprotein particle metabolites depending on their size (upper row) or density (lower row). The coefficients represent the change associated with hospitalization, death and disease severity. (B) Volcano plot of clinical variables associated with COVID-19 severity in our cohort. (C) Distribution of clinical parameters in the samples dependent of COVID-19 severity. The horizontal grey areas represent a healthy range for each parameter.

REFERENCES

- John Hopkins University Coronavirus Resource Center. Available at: <https://coronavirus.jhu.edu/> (Accessed July 15, 2021).
- Sinha P, Calfee CS, Cherian S, Brealey D, Cutler S, King C, et al. Prevalence of Phenotypes of Acute Respiratory Distress Syndrome in Critically Ill Patients With COVID-19: A Prospective Observational Study. *Lancet Respir Med* (2020). doi: 10.1016/S2213-2600(20)30366-0
- Yang J, Zheng Y, Gou X, Pu K, Chen Z, Guo Q, et al. Prevalence of Comorbidities and its Effects in Patients Infected With SARS-CoV-2: A Systematic Review and Meta-Analysis. *Int J Infect Dis* (2020) 94:91–5. doi: 10.1016/j.ijid.2020.03.017
- Zhou F, Yu T, Du R, Fan G, Liu Y, Liu Z, et al. Clinical Course and Risk Factors for Mortality of Adult Inpatients With COVID-19 in Wuhan, China: A Retrospective Cohort Study. *Lancet* (2020) 395:1054–62. doi: 10.1016/S0140-6736(20)30566-3
- Grasselli G, Tonetti T, Protti A, Langer T, Girardis M, Bellani G, et al. Pathophysiology of COVID-19-Associated Acute Respiratory Distress Syndrome: A Multicentre Prospective Observational Study. *Lancet Respir Med* (2020). doi: 10.1016/S2213-2600(20)30370-2
- Guan W-J, Ni Z-Y, Hu Y, Liang W-H, Ou C-Q, He J-X, et al. Clinical Characteristics of Coronavirus Disease 2019 in China. *N Engl J Med* (2020) 382:1708–20. doi: 10.1056/NEJMoa2002032
- Huang C, Wang Y, Li X, Ren L, Zhao J, Hu Y, et al. Clinical Features of Patients Infected With 2019 Novel Coronavirus in Wuhan, China. *Lancet* (2020) 395:497–506. doi: 10.1016/S0140-6736(20)30183-5
- Huang J, Cheng A, Kumar R, Fang Y, Chen G, Zhu Y, et al. Hypoalbuminemia Predicts the Outcome of COVID-19 Independent of Age and Co-Morbidity. *J Med Virol* (2020) 92:2152–8. doi: 10.1002/jmv.26003
- Richardson S, Hirsch JS, Narasimhan M, Crawford JM, McGinn T, Davidson KW, et al. Presenting Characteristics, Comorbidities, and Outcomes Among 5700 Patients Hospitalized With COVID-19 in the New York City Area. *JAMA* (2020). doi: 10.1001/jama.2020.6775
- Shi Y, Tan M, Chen X, Liu Y, Huang J, Ou J, et al. Immunopathological Characteristics of Coronavirus Disease 2019 Cases in Guangzhou, China. *medRxiv* (2020), 2020.03.12.20034736. doi: 10.1101/2020.03.12.20034736
- Wang W, Su B, Pang L, Qiao L, Feng Y, Ouyang Y, et al. High-Dimensional Immune Profiling by Mass Cytometry Revealed Immunosuppression and Dysfunction of Immunity in COVID-19 Patients. *Cell Mol Immunol* (2020) 17:650–2. doi: 10.1038/s41423-020-0447-2
- Wang G, Wu C, Zhang Q, Wu F, Yu B, Lv J, et al. C-Reactive Protein Level May Predict the Risk of COVID-19 Aggravation. *Open Forum Infect Dis* (2020) 7:ofaa153. doi: 10.1093/ofid/ofaa153
- Wang H, Yuan Z, Pavel MA, Jablonski SM, Jablonski J, Hobson R, et al. The Role of High Cholesterol in Age-Related COVID19 Lethality. *bioRxiv* (2020). doi: 10.1101/2020.05.09.086249
- Tay MZ, Poh CM, Rénia L, MacAry PA, Ng LFP. The Trinity of COVID-19: Immunity, Inflammation and Intervention. *Nat Rev Immunol* (2020) 20:363–74. doi: 10.1038/s41577-020-0311-8
- Hennigan S, Kavanaugh A. Interleukin-6 Inhibitors in the Treatment of Rheumatoid Arthritis. *Ther Clin Risk Manage* (2008) 4:767–75. doi: 10.2147/tcrm.s3470
- Guaraldi G, Meschiari M, Cozzi-Lepri A, Milic J, Tonelli R, Menozzi M, et al. Tocilizumab in Patients With Severe COVID-19: A Retrospective Cohort Study. *Lancet Rheumatol* (2020) 2:e474–84. doi: 10.1016/S2665-9913(20)30173-9
- Xu G, Qi F, Li H, Yang Q, Wang H, Wang X, et al. The Differential Immune Responses to COVID-19 in Peripheral and Lung Revealed by Single-Cell RNA Sequencing. *medRxiv* (2020). doi: 10.1101/2020.08.15.20175638
- Wilk AJ, Rustagi A, Zhao NQ, Roque J, Martínez-Colón GJ, McKechnie JL, et al. A Single-Cell Atlas of the Peripheral Immune Response in Patients With Severe COVID-19. *Nat Med* (2020) 1–7. doi: 10.1038/s41591-020-0944-y
- Agrati C, Sacchi A, Bordoni V, Cimmini E, Notari S, Grassi G, et al. Expansion of Myeloid-Derived Suppressor Cells in Patients With Severe Coronavirus Disease (COVID-19). *Cell Death Differ* (2020). doi: 10.1038/s41418-020-0572-6
- Tan L, Wang Q, Zhang D, Ding J, Huang Q, Tang Y-Q, et al. Lymphopenia Predicts Disease Severity of COVID-19: A Descriptive and Predictive Study. *Signal Transduct Target Ther* (2020) 5:33. doi: 10.1038/s41392-020-0148-4
- Ye Q, Wang B, Mao J. The Pathogenesis and Treatment of the 'Cytokine Storm' in COVID-19. *J Infection* (2020) 80:607–13. doi: 10.1016/j.jinf.2020.03.037
- Nicolai L, Leunig A, Brambs S, Kaiser R, Weinberger T, Weigand M, et al. Immunothrombotic Dysregulation in COVID-19 Pneumonia Is Associated With Respiratory Failure and Coagulopathy. *Circulation* (2020) 142:1176–89. doi: 10.1161/CIRCULATIONAHA.120.048488
- Takahashi T, Wong P, Ellingson M, Lucas C, Klein J, Israelow B, et al. Sex Differences in Immune Responses to SARS-CoV-2 That Underlie Disease Outcomes. *Nature* (2020) 588:315–20. doi: 10.1038/s41586-020-2700-3
- Lucas C, Wong P, Klein J, Castro TBR, Silva J, Sundaram M, et al. Longitudinal Analyses Reveal Immunological Misfiring in Severe COVID-19. *Nature* (2020) 584:463–9. doi: 10.1038/s41586-020-2588-y
- Dierckx T, van Elslande J, Salmela H, Decru B, Wauters E, Gunst J, et al. The Metabolic Fingerprint of COVID-19 Severity. *bioRxiv* (2020). doi: 10.1101/2020.11.09.20228221
- Blasco H, Bessy C, Plantier L, Lefevre A, Piver E, Bernard L, et al. The Specific Metabolome Profiling of Patients Infected by SARS-CoV-2 Supports the Key Role of Tryptophan-Nicotinamide Pathway and Cytosine Metabolism. *Sci Rep* (2020) 10:16824. doi: 10.1038/s41598-020-73966-5
- Geyer PE, Arend FM, Doll S, Louiset M-L, Virreira Winter S, Müller-Reif JB, et al. High-Resolution Serum Proteome Trajectories in COVID-19 Reveal Patient-Specific Seroconversion. *EMBO Mol Med* (2021), e14167. doi: 10.15252/emmm.202114167

28. Meoni G, Ghini V, Maggi L, Vignoli A, Mazzoni A, Salvati L, et al. Metabolomic/lipidomic Profiling of COVID-19 and Individual Response to Tocilizumab. *PLoS Pathog* (2021) 17:e1009243. doi: 10.1371/journal.ppat.1009243
29. Danlos F-X, Grajeda-Iglesias C, Durand S, Sauvat A, Roumier M, Cantin D, et al. Metabolomic Analyses of COVID-19 Patients Unravel Stage-Dependent and Prognostic Biomarkers. *Cell Death Dis* (2021) 12:258. doi: 10.1038/s41419-021-03540-y
30. Chazal N, Gerlier D. Virus Entry, Assembly, Budding, and Membrane Rafts. *Microbiol Mol Biol Rev* (2003) 67:226–37. doi: 10.1128/MMBR.67.2.226-237.2003
31. Mazzon M, Mercer J. Lipid Interactions During Virus Entry and Infection. *Cell Microbiol* (2014) 16:1493–502. doi: 10.1111/cmi.12340
32. Welte MA, Gould AP. Lipid Droplet Functions Beyond Energy Storage. *Biochim Biophys Acta Mol Cell Biol Lipids* (2017) 1862:1260–72. doi: 10.1016/j.bbalip.2017.07.006
33. Watson RR, Demeester F. *Handbook of Lipids in Human Function: Fatty Acids*. Elsevier (2015). Available at: <https://play.google.com/store/books/details?id=jdM4CgAAQBAJ>.
34. Song J-W, Lam SM, Fan X, Cao W-J, Wang S-Y, Tian H, et al. Omics-Driven Systems Interrogation of Metabolic Dysregulation in COVID-19 Pathogenesis. *Cell Metab* (2020) 32:188–202.e5. doi: 10.1016/j.cmet.2020.06.016
35. Lee W, Ahn JH, Park HH, Kim HN, Kim H, Yoo Y, et al. COVID-19-Activated SREBP2 Disturbs Cholesterol Biosynthesis and Leads to Cytokine Storm. *Signal Transduct Target Ther* (2020) 5:186. doi: 10.1038/s41392-020-00292-7
36. Ahola-Olli AV, Mustelin L, Kalimeri M, Kettunen J, Jokelainen J, Auvinen J, et al. Circulating Metabolites and the Risk of Type 2 Diabetes: A Prospective Study of 11,896 Young Adults From Four Finnish Cohorts. *Diabetologia* (2019) 62:2298–309. doi: 10.1007/s00125-019-05001-w
37. Tikkanen E, Jägerroos V, Rodosthenous R, Holmes M, Sattar N, Ala-Korpela M, et al. Metabolic Biomarkers for Peripheral Artery Disease Compared With Coronary Artery Disease: Lipoprotein and Metabolite Profiling of 31,657 Individuals From Five Prospective Cohorts. *bioRxiv* (2020). doi: 10.1101/2020.07.24.20158675
38. Nightingale Health UK Biobank Initiative, Julkunen H, Cichonska A, Slagboom PE, Würtz P. Blood Biomarker Score Identifies Individuals at High Risk for Severe COVID-19 a Decade Prior to Diagnosis: Metabolic Profiling of 105,000 Adults in the UK Biobank. *bioRxiv* (2020). doi: 10.1101/2020.07.02.20143685
39. Nightingale Health UK Biobank Initiative, Julkunen H, Cichonska A, Slagboom PE, Würtz P. Metabolic Biomarker Profiling for Identification of Susceptibility to Severe Pneumonia and COVID-19 in the General Population. *Elife* (2021) 10. doi: 10.7554/eLife.63033
40. World Health Organization. *WHO R&D Blueprint: Novel Coronavirus COVID-19 Therapeutic Trial Synopsis*. Available at: www.who.int/blueprint/priority-diseases/key-action/COVID-19_Treatment_Trial_Design_Master_Protocol_synopsis_Final_18022020.pdf (Accessed July 15, 2021).
41. Corti MC, Guralnik JM, Salive ME, Sorkin JD. Serum Albumin Level and Physical Disability as Predictors of Mortality in Older Persons. *JAMA* (1994) 272:1036–42. doi: 10.1001/jama.1994.03520130074036
42. Vaidya VS, Ferguson MA, Bonventre JV. Biomarkers of Acute Kidney Injury. *Annu Rev Pharmacol Toxicol* (2008) 48:463–93. doi: 10.1146/annurev.pharmtox.48.113006.094615
43. Barski R. Lipids, Lipoproteins, and Apolipoproteins as Risk Markers of Myocardial Infarction in 52 Countries (the INTERHEART Study): A Case-Control Study. *Ann Clin Biochemistry: Int J Lab Med* (2009) 46:266–6. doi: 10.1258/acb.2009.200903
44. Ritchie SC, Würtz P, Nath AP, Abraham G, Havulinna AS, Fearnley LG, et al. The Biomarker GlycA Is Associated With Chronic Inflammation and Predicts Long-Term Risk of Severe Infection. *Cell Syst* (2015) 1:293–301. doi: 10.1016/j.cels.2015.09.007
45. Sudlow C, Gallacher J, Allen N, Beral V, Burton P, Danesh J, et al. UK Biobank: An Open Access Resource for Identifying the Causes of a Wide Range of Complex Diseases of Middle and Old Age. *PLoS Med* (2015) 12:e1001779. doi: 10.1371/journal.pmed.1001779
46. Masana L, Correig E, Ibarretxe D, Anoro E, Arroyo JA, Jericó C, et al. Low HDL and High Triglycerides Predict COVID-19 Severity. *Sci Rep* (2021) 11:7217. doi: 10.1038/s41598-021-86747-5
47. Alfano CM, Imayama I, Neuhaus ML, Kiecolt-Glaser JK, Smith AW, Meeske K, et al. Fatigue, Inflammation, and ω -3 and ω -6 Fatty Acid Intake Among Breast Cancer Survivors. *J Clin Oncol* (2012) 30:1280–7. doi: 10.1200/JCO.2011.36.4109
48. Simopoulos AP. The Importance of the Ratio of Omega-6/Omega-3 Essential Fatty Acids. *Biomed Pharmacother* (2002) 56:365–79. doi: 10.1016/s0753-3322(02)00253-6
49. Hubler MJ, Kennedy AJ. Role of Lipids in the Metabolism and Activation of Immune Cells. *J Nutr Biochem* (2016) 34:1–7. doi: 10.1016/j.jnutbio.2015.11.002
50. Almeida L, Lochner M, Berod L, Sparwasser T. Metabolic Pathways in T Cell Activation and Lineage Differentiation. *Semin Immunol* (2016) 28:514–24. doi: 10.1016/j.smim.2016.10.009
51. Rathmell JC, Vander Heiden MG, Harris MH, Frauwirth KA, Thompson CB. In the Absence of Extrinsic Signals, Nutrient Utilization by Lymphocytes Is Insufficient to Maintain Either Cell Size or Viability. *Mol Cell* (2000) 6:683–92. doi: 10.1016/s1097-2765(00)00066-6
52. Roos D, Loos JA. Changes in the Carbohydrate Metabolism of Mitogenically Stimulated Human Peripheral Lymphocytes. II. Relative Importance of Glycolysis and Oxidative Phosphorylation on Phytohemagglutinin Stimulation. *Exp Cell Res* (1973) 77:127–35. doi: 10.1016/0014-4827(73)90561-2
53. Frauwirth KA, Riley JL, Harris MH, Parry RV, Rathmell JC, Plas DR, et al. The CD28 Signaling Pathway Regulates Glucose Metabolism. *Immunity* (2002) 16:769–77. doi: 10.1016/s1074-7613(02)00323-0
54. Hardardóttir I, Grünfeld C, Feingold KR. Effects of Endotoxin and Cytokines on Lipid Metabolism. *Curr Opin Lipidol* (1994) 5:207–15. doi: 10.1097/00041433-199405030-00008
55. Grunfeld C, Feingold KR. Regulation of Lipid Metabolism by Cytokines During Host Defense. *Nutrition* (1996) 12:S24–6. doi: 10.1016/0899-9007(96)90013-1
56. Rendeiro AF, Casano J, Vorkas CK, Singh H, Morales A, DeSimone RA, et al. Profiling of Immune Dysfunction in COVID-19 Patients Allows Early Prediction of Disease Progression. *Life Sci Alliance* (2021) 4:e202000955. doi: 10.26508/lsa.202000955
57. Rendeiro AF, Ravichandran H, Bram Y, Chandar V, Kim J, Meydan C, et al. The Spatial Landscape of Lung Pathology During COVID-19 Progression. *Nature* (2021) 593:564–9. doi: 10.1038/s41586-021-03475-6
58. Carpintero R, Gruaz L, Brandt KJ, Scanu A, Faille D, Combes V, et al. HDL Interfere With the Binding of T Cell Microparticles to Human Monocytes to Inhibit Pro-Inflammatory Cytokine Production. *PLoS One* (2010) 5:e11869. doi: 10.1371/journal.pone.0011869
59. Rader DJ. High-Density Lipoproteins and Atherosclerosis. *Am J Cardiol* (2002) 90. doi: 10.1016/s0002-9149(02)02635-8
60. Borén J, Chapman MJ, Krauss RM, Packard CJ, Bentzon JF, Binder CJ, et al. Low-Density Lipoproteins Cause Atherosclerotic Cardiovascular Disease: Pathophysiological, Genetic, and Therapeutic Insights: A Consensus Statement From the European Atherosclerosis Society Consensus Panel. *Eur Heart J* (2020) 41:2313–30. doi: 10.1093/eurheartj/ehz962
61. Mundi S, Massaro M, Scoditti E, Carluccio MA, van Hinsbergh VWM, Iruela-Arispe ML, et al. Endothelial Permeability, LDL Deposition, and Cardiovascular Risk Factors—A Review. *Cardiovasc Res* (2018) 114:35–52. doi: 10.1093/cvr/cvx226
62. Ackermann M, Verleden SE, Kuehnel M, Haverich A, Welte T, Laenger F, et al. Pulmonary Vascular Endothelialitis, Thrombosis, and Angiogenesis in Covid-19. *N Engl J Med* (2020) NEJMoa2015432. doi: 10.1056/NEJMoa2015432
63. Zuo Y, Estes SK, Ali RA, Gandhi AA, Yalavarthi S, Shi H, et al. Prothrombotic Autoantibodies in Serum From Patients Hospitalized With COVID-19. *Sci Transl Med* (2020) 12. doi: 10.1126/scitranslmed.abd3876
64. Thematic Review Series: The Pathogenesis of Atherosclerosis. Effects of Infection and Inflammation on Lipid and Lipoprotein Metabolism Mechanisms and Consequences to the Host. *J Lipid Res* (2004) 45:1169–96. doi: 10.1194/jlr.R300019-JLR200
65. Horejsi V. Lipid Rafts and Their Roles in T-Cell Activation. *Microbes Infect* (2005) 7:310–6. doi: 10.1016/j.micinf.2004.12.004
66. Kim W, Khan NA, McMurray DN, Prior IA, Wang N, Chapkin RS. Regulatory Activity of Polyunsaturated Fatty Acids in T-Cell Signaling. *Prog Lipid Res* (2010) 49:250–61. doi: 10.1016/j.plipres.2010.01.002
67. Kim S-Y, Volsky DJ. PAGE: Parametric Analysis of Gene Set Enrichment. *BMC Bioinf* (2005) 6:144. doi: 10.1186/1471-2105-6-144

68. Lamerton RE, Lightfoot A, Nieves DJ, Owen DM. The Role of Protein and Lipid Clustering in Lymphocyte Activation. *Front Immunol* (2021) 12:600961. doi: 10.3389/fimmu.2021.600961
69. Veglia F, Tyurin VA, Blasi M, De Leo A, Kossenkov AV, Donthireddy L, et al. Fatty Acid Transport Protein 2 Reprograms Neutrophils in Cancer. *Nature* (2019) 569:73–8. doi: 10.1038/s41586-019-1118-2
70. Soininen P, Kangas AJ, Würtz P, Tuikainen T, Tynkkynen T, Laatikainen R, et al. High-Throughput Serum NMR Metabonomics for Cost-Effective Holistic Studies on Systemic Metabolism. *Analyst* (2009) 134:1781–5. doi: 10.1039/b910205a
71. Soininen P, Kangas AJ, Würtz P, Suna T, Ala-Korpela M. Quantitative Serum Nuclear Magnetic Resonance Metabolomics in Cardiovascular Epidemiology and Genetics. *Circ Cardiovasc Genet* (2015) 8:192–206. doi: 10.1161/CIRCGENETICS.114.000216
72. Wolf FA, Angerer P, Theis FJ. SCANPY: Large-Scale Single-Cell Gene Expression Data Analysis. *Genome Biol* (2018) 19:15. doi: 10.1186/s13059-017-1382-0
73. van der Maaten L, Hinton G. Visualizing Data Using T-SNE. *J Mach Learn Res* (2008) 9:2579–605.
74. Agrawal A, Ali A, Boyd S. Minimum-Distortion Embedding. *arXiv [cs.LG]* (2021). Available at: <http://arxiv.org/abs/2103.02559>.
75. Bilenko NY, Gallant JL. Pyrrca: Regularized Kernel Canonical Correlation Analysis in Python and Its Applications to Neuroimaging. *Front Neuroinform* (2016) 10:49. doi: 10.3389/fninf.2016.00049
76. Harris CR, Millman KJ, van der Walt SJ, Gommers R, Virtanen P, Cournapeau D, et al. Array Programming With NumPy. *Nature* (2020) 585:357–62. doi: 10.1038/s41586-020-2649-2
77. Virtanen P, Gommers R, Oliphant TE, Haberland M, Reddy T, Cournapeau D, et al. SciPy 1.0: Fundamental Algorithms for Scientific Computing in Python. *Nat Methods* (2020) 17:261–72. doi: 10.1038/s41592-019-0686-2
78. Seabold S, Perktold J. (2010). Statsmodels: Econometric and Statistical Modeling With Python, In: *Proceedings of the 9th Python in Science Conference*. doi: 10.25080/majora-92bf1922-011
79. Pedregosa F, Varoquaux G. Scikit-Learn: Machine Learning in Python. *J Mach Learn Res* (2011) 12:2825–30. doi: 10.5555/1953048.2078195
80. Vallat R. Pingouin: Statistics in Python. *JOSS* (2018) 3:1026. doi: 10.21105/joss.01026

Conflict of Interest: OE is scientific advisor and equity holder in Freenome, Owkin, Volastra Therapeutics and OneThree Biotech.

The remaining authors declare that the research was conducted in the absence of any commercial or financial relationships that could be construed as a potential conflict of interest.

Publisher's Note: All claims expressed in this article are solely those of the authors and do not necessarily represent those of their affiliated organizations, or those of the publisher, the editors and the reviewers. Any product that may be evaluated in this article, or claim that may be made by its manufacturer, is not guaranteed or endorsed by the publisher.

Copyright © 2022 Rendeiro, Vorkas, Krumsiek, Singh, Kapadia, Cappelli, Cacciapuoti, Inghirami, Elemento and Salvatore. This is an open-access article distributed under the terms of the Creative Commons Attribution License (CC BY). The use, distribution or reproduction in other forums is permitted, provided the original author(s) and the copyright owner(s) are credited and that the original publication in this journal is cited, in accordance with accepted academic practice. No use, distribution or reproduction is permitted which does not comply with these terms.